Heliyon 10 (2024) e37283

Contents lists available at ScienceDirect

Heliyon

journal homepage: www.cell.com/heliyon

Research article

Berberine-loaded nanoemulsions as a natural food preservative; the impact of femtosecond laser irradiation on the antibacterial activity

Liana Parseghian [a,b], Nastaran Kahrarian [c], Atoosa Sadat Arabanian [c,*], Zinab Moradi Alvand [a,b], Reza Massudi [c], Masoud Rahimi [b], Hasan Rafati [b,**]

[a] Department of Phytochemistry, Medicinal Plants and Drugs Research Institute, Shahid Beheshti University, Tehran, Iran
[b] Department of Pharmaceutical Engineering, Medicinal Plants and Drugs Research Institute, Shahid Beheshti University, Tehran, Iran
[c] Department of Laser and Plasma Research Institute, Shahid Beheshti University, Tehran, Iran

ARTICLE INFO

Keywords:
Femtosecond laser pulses
Surface modification
Berberine
Nanoemulsion
Antibacterial activity

ABSTRACT

There is a growing concern among food safety regulators, the food industry, and consumers about foodborne illnesses. To improve food safety and increase shelf life, it is necessary to use natural preservatives. Natural antimicrobials are safer than artificial preservatives because they can prevent microbial resistance while also meeting consumers' demands for healthier food. This study used Berberine to enhance the antibacterial activity of *Satureja Khuzistanica* essential oil nanoemulsions (SKEO NE) against *Staphylococcus aureus* (*S. aureus*) bacteria, making them a promising option as preservatives. Response Surface Methodology (RSM) was employed to determine the optimized Berberine loaded SKEO NE (Berberine/SKEO NE), resulting in a mean droplet size of 88.60 nm at 6.91, 3.21, and 0.08% w/w of surfactant, essential oil, and Berberine, respectively. Berberine utilization in SKEO NE has led to an increase in antibacterial activity. The nanoemulsion samples significantly ruptured the *S. aureus* bacterial cell membrane, rapidly discharging cell contents. The use of a microfluidic system in tandem based on the conventional approach significantly accelerated this process. Enhancing the interaction between nanodroplets and the bacterial membrane can be achieved through the nanoemulsification process of EOs, which involves modifying their surface characteristics. This enhancement is particularly pronounced when employing microfluidic systems due to their substantial contact surface area. We investigated the potential of using femtosecond laser irradiation at a wavelength of 1040 nm to augment the antibacterial action of nanoemulsions. The combined treatment of laser and nanoemulsions significantly increased the antibacterial effect of nanoemulsions by approximately 15% for each bacterium, suggesting the potential utility of this treatment to bolster the antibacterial activity of nanoemulsions. Bacteria were trapped using optical tweezers for up to 20 min, with bacterial destruction observed starting at 3 min and exhaustive destruction evident after 20 min.

* Corresponding author.
** Corresponding author.
E-mail addresses: a_arabanian@sbu.ac.ir (A.S. Arabanian), h_rafati@sbu.ac.ir (H. Rafati).

https://doi.org/10.1016/j.heliyon.2024.e37283
Received 9 June 2024; Received in revised form 29 August 2024; Accepted 30 August 2024
Available online 3 September 2024

1. Introduction

Food preservation is critical for maintaining food's health over extended periods. Fundamentally, inhibiting harmful microbe growth enables food preservation [1]. For the inactivation of contaminant bacteria, both chemical and physical approaches are available, such as non-thermal plasma (NTP), which employs plasma multi-jets as an effective bactericidal agent [2]. However, organic preservatives are preferred over chemical ones for several reasons. Firstly, they are more effective in preventing biodegradation as they are less likely to be transformed by microorganisms in soil and wood. Moreover, studies have shown that natural preservatives extracted from plants are highly effective in inhibiting bacterial growth and preventing food spoilage. They also offer additional health benefits [3]. For example, excessive consumption of artificial preservatives, regardless of their source, can lead to various health problems such as gastroesophageal reflux disease [4]. In response to the food industry's need for natural antibacterial agents, there has been a growing interest in natural additives. Natural preservatives in processed foods are highly sought after because they are considered safer and more beneficial for public health than chemical alternatives [5].

Plant chemicals, particularly alkaloids, coumarins, and tannins, appear to be effective antimicrobials in food applications, each employing a distinct mechanism of action due to structural variations [6]. *Satureja khuzistanica* essential oil (SKEO), rich in carvacrol, has been used in numerous research projects for therapeutic and food preservative purposes because of its anti-inflammatory, antibacterial, antioxidant, and anticancer properties [7]. One of the plant-derived substances that has been discovered is Berberine. It is a quaternary alkaloid that is widely known for its antibacterial effects [8]. Unlike antibiotics such as Neomycin, Berberine rarely induces bacterial resistance mutations. Both gram-positive and gram-negative bacterial strains were susceptible to the antibacterial effects of Berberine [9]. By extension, it exhibits a significant direct antibacterial action that furthers the ability to regulate host immunity [10]. Despite its antibacterial properties, Berberine is not currently utilized as a feed additive or preservative, and its preservative qualities remain unexplored [11]. Research led by Kaya et al. demonstrated that chitosan-fruit extract film incorporating *B. crataegina* fruit extract, as a source of Berberine, could enhance the physicochemical, antibacterial, and biological properties of edible films compared to chitosan film alone explored Berberine's potential as a feed additive for animal nutrition, noting its extensive pharmacological properties. They also highlighted its maximum oral ingestion range across various feed types due to potential toxicity [12]. Berberine shows promise for novel antibiotic development due to its capability to inhibit antibiotic-resistant bacteria [13], compared to other methods like NTP, which involves plasma treatment that reduces both bacterial adhesion and viability [2]. Recent research indicates Berberine's ability to disrupt methicillin-resistant *S. aureus* (MRSA) cell walls and membranes, synergizing with clindamycin or rifamycin to eradicate bacteria [14].

However, Berberine's limited water solubility hampers its dissolution rate and oral bioavailability, constraining its therapeutic utility [15]. Thus, developing a novel drug delivery mechanism is imperative to enhance its delivery and bioavailability [16]. Various nanoencapsulation techniques suitable for food preservation exist, including edible films, solid lipid nanoparticles, nanofibers, and nanoemulsions [17]. Nanoemulsion is the most popular and efficient among these techniques due to its heightened surface-to-volume ratio. It facilitates enhanced molecular interactions with bacterial cell surfaces, producing more substantial antibacterial effects [18].

Considering the reasons discussed earlier, nanoemulsions would likely enhance the antibacterial efficacy by loading Berberine into SKEO. Additionally, these properties can be assessed using microfluidic systems as a tool for microscale fluid flow, providing a large contact area for observing the interaction between nanoparticles and bacteria [19].

The primary challenge in accomplishing this objective would involve manipulating and controlling the target cells while increasing the likelihood of interactions within shorter time frames. This would enable researchers to study factors such as cell responses to different chemicals qualitatively and quantitatively [20].

For this purpose, Optical tweezers offer considerable potential. Traditionally, they have been used for single-molecule investigations, such as exploring the interaction between DNA and helicases or repair complexes [21]. Optical tweezers have also found applications in microbiological research, including cell sorting in microfluidics, investigating cellular responses to rapid cell switching between media, and disaggregating cell clusters in biofilm studies [22]. Additionally, optical trapping of individual bacteria is utilized to observe flagellar motion using fluorescence microscopy to characterize changes in cell movement [23], to assess cell viability under environmental changes [24], and to investigate cellular responses to flagellar rotation inhibition [25]. It is essential to consider the operational characteristics of the laser, such as fluence, wavelength, and energy, to minimize potential unintended disruptions, such as reactive oxygen species production, from optical tweezers [26]. Optical tweezers capture cells, allowing observation of any temporal morphological changes when treated with formulations [27].

Femtosecond laser pulses can create minuscule openings in the cell surface, facilitating easier entry of substances into the cell and increasing the permeability of the cell wall to nanoemulsions, thus accelerating bacterial death [28].

Such laser pulses are also believed to be able to finely manipulate the states of living cells by creating pores of different sizes through laser power adjustments [29].

The primary objective of the current study was to assess the feasibility of producing a stable Berberine/SKEO NE and to investigate the impact of various formulation concentrations on bacterial cells by trapping *S. aureus* bacteria and observing potential morphological alterations. More importantly, femtosecond laser pulses are employed to illuminate trapped cells in Berberine/SKEO NE to confirm any potential effects on the rate of morphological changes in cells and the enhanced effect of nanoemulsion on bacteria due to potential cell wall debilitation. Consequently, the degree of bacterial cell disruption in shorter durations is observed, highlighting the beneficial roles of femtosecond laser pulse irradiation.

2. Materials and instruments

2.1. Materials

Khorraman Pharmaceutical Co. supplied Pure SKEO. Merck Millipore (Darmstadt, Germany) provided Tween 80 and Span 80. Photoconductors SU-8 and polydimethylsiloxane (PDMS) were obtained from MicroChem and Dow Corning for microchannel fabrication. *S. aureus* (ATCC6538) from Pasteur Institute of Iran, and Nutrient agar, Mueller Hinton Broth (MHB), Luria Bertani Broth (LB), and Mueller Hinton Agar (MHA) were purchased from CONDA Pronadisa.

2.2. Instruments

A syringe pump (Safir Soraya, Iran) was utilized for substance injection. Transmission Electron Microscopy (TEM) (Philips-CM30), Scanning Electron Microscopy (SEM) (JEOL, Japan), a Dynamic Light Scattering (DLS) device (Nanophox Sympatec GmbH, Clausthal, Germany), a high-speed homogenizer (SilentCrusher M, Heidolph, Germany), a UV–visible spectrophotometer (Bio-photometer, Eppendorf AG, Hamburg, Germany), and an atomic absorption spectrophotometer (Analytik Jena, ContrAA700, Jena, Germany) were the instruments utilized for further evaluation in the present study.

2.3. Experimental design

The conventional optimization approach employing the one-factor-at-a-time (OFAT) strategy is time-consuming, labor-intensive, and costly. Additionally, the approach lacks insights into the intricate interactions among different process variables and their effects on the outcome. Therefore, we utilized Design of Experiments (DoE), a statistical approach, to optimize technological processes. Orthogonal array design, Box-Behnken Design (BBD), and Central Composite Design (CCD) are among the most widely used DoE strategies for identifying optimal operating variables. Since each variable in Design Expert software requires low and high values, we first conducted several experiments and preliminary testing to find out the best and most appropriate ranges as follows: Surfactant 3.0%, 5.0%, 7.0% w/w; essential oil 3.0%, 4.0%, 5.0% w/w; and Berberine 0.06%, 0.08%, 0.10% w/w. We conducted 17 trials corresponding to BBD, including five replications of the center point, to accurately assess the statistical error (Table S1). We also utilized Equation (1), a quadratic regression model, to predict the relationship between the factors and the size of the nanoemulsion droplets:

$$Y = \beta_0 + \beta_1 X_1 + \beta_2 X_2 + \beta_3 X_3 + \beta_{12} X_1X_2 + \beta_{13} X_1X_3 + \beta_{23} X_2X_3 + \beta_{11}X_1^2 + \beta_{22}X_2^2 + \beta_{33}X_3^2 \quad (1)$$

Where Y denotes the droplet size (nm); β_0 is the intercept coefficient; β_1, β_2 and β_3 are the linear coefficients; β_{11}, β_{22}, and β_{33} are the squared coefficients; and the interactive coefficients are β_12, β_13, and β_23 (utilizing Design-Expert software). The trial results were analyzed using Design-Expert software (State-Ease Inc., version 7.0.0).

2.4. Preparation of Berberine/SKEO NE and stability evaluation

The Berberine/SKEO NE was prepared as follows. It comprised a specific mixture of SKEO, surfactants, and Berberine. Berberine, SKEO, and Span 80 were mixed with a Tween 80 solution in deionized water. The mixture was homogenized using a high-speed homogenizer for 20 min while swirling at 15,000 rpm. The stability of the resulting nanoemulsions was evaluated over 65 days at room temperature and in a refrigerator by measuring the average particle diameter simultaneously.

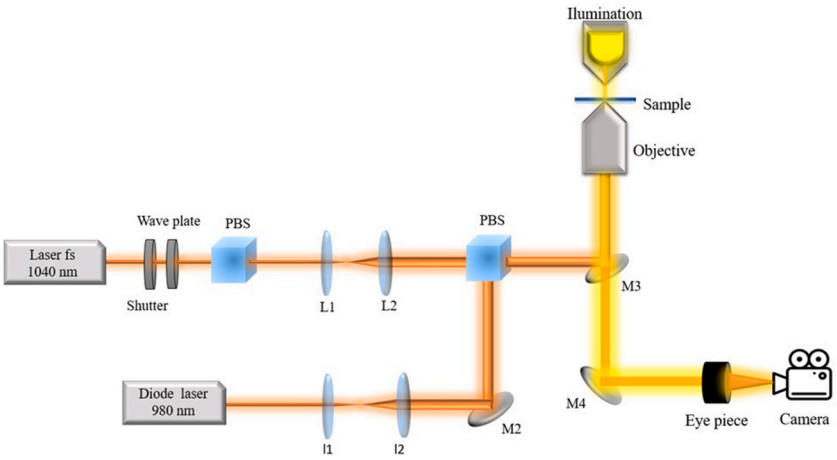

Fig. 1. Schematic diagram of the experimental setup.

2.5. Experimental optical Set-up

A homemade femtosecond fiber laser that delivers 200-fs pulses at 1040 nm with a maximum energy of 5 nJ per pulse and a repetition rate of 23-MHz was used as the light source for creating transient openings in the cell plasma membrane. In biological research, femtosecond laser pulses are used as a scalpel because they can provide high peak powers with low pulse energy. The experimental setup is depicted schematically in Fig. 1. The laser beam spot diameter was enlarged using a Galilean telescope with plano-concave and plano-convex lenses, with focal lengths of 50 mm and 250 mm, respectively, to match the effective aperture behind the objective lens. A half-wave plate and a polarizing beam splitter were positioned in the laser beam path to adjust its intensity, and a mechanical shutter regulated the laser beam's exposure time. An optical laser tweezer was made using a continuous wave diode laser (@980 nm) to trap and control cells in situ. Bacterial cells were typically trapped utilizing a diode laser power of 35–45 mW. The diode laser beam was aligned collinearly with the femtosecond laser beam using the second polarizing beam splitter. Both laser beams entered the inverted microscope through the M2 mirror and focused on the sample with an oil-immersed objective lens having a magnification of 100X and a numerical aperture of 1.25. Samples were positioned on a coverslip mounted on a manual x-y-z three-axis stage. An LED and a 10X objective lens provided illumination for the microscope. The M3 mirror directed the visible light of the microscope illumination to a 10X magnification eyepiece. All images were captured using a camera placed at the focal plane of the eyepiece. Perforation and destruction of bacterial cell surfaces were achieved by illuminating the target with femtosecond laser pulses with energies ranging from 0.6 nJ to 0.65 nJ per pulse. The pulse energy of the femtosecond laser and the power of the diode laser were optimized to ensure that the viability of the bacteria was not compromised.

2.6. Microfluidic fabrication and experimental setup

The microfluidic setup is demonstrated in our previous work [30]. Briefly, the microchannel constructed of PDMS (Dow Corning Crop, USA) was formed utilizing the microlithography process. The master molds were created using photolithography with SU-8 photoresist film. The PDMS liquid (Sylgard 184) and PDMS curing agent were then carefully combined in a 10:1 ratio before pouring into the SU-8 molds. After 30 min of treatment at 90°C, PDMS separated from the molds. Finally, the oxygen plasma method was utilized to bond the two PDMS layers for 1 min at 8 mbar and 40 W. A biopsy punch with a width of 1.25 mm was used to produce inlets and outlets for microchannels.

It should be emphasized that the constructed microfluidic system had been sterilized with 70% ethanol before testing. Nanoemulsion samples and culture media (MHB) at various concentrations were constantly pumped into the inlets via a syringe pump.

2.7. Preparation of S. aureus bacterium

Gram-positive (*S. aureus*) bacterial strains were employed to assess the antibacterial efficacy of the conventional approach and the nanoemulsion within the microfluidic system. The bacteria were cultured on Mueller-Hinton agar for a full day at 37°C [31]. Subsequently, a colony was selected and cultured in a sterilized Nutrient Broth (NB) medium following a 2-h incubation at 37°C and 250 rpm. The absorption was measured at a wavelength of 600 nm (OD_{600} nm equals 0.400), indicating bacterial growth. The bacterial suspension was utilized for the conventional evaluation method and injection into the microfluidic channel.

2.8. Minimum inhibitory concentration (MIC) and minimum bactericidal concentration (MBC) tests

Determining MIC and MBC was the initial step in evaluating the antibacterial activity of NE. MIC referred to the lowest concentration of the test agent that inhibited growth on agar. At the same time, MBC denoted the lowest concentration of the compound, which kills the bacteria. Typically, MBC values exceeded MIC values. NE was serially diluted in sterile MHB in microtiter wells. Subsequently, 25 μL of standardized cell suspension (10^7 CFU/mL) was added to each well and incubated overnight at 37°C [32]. The MIC was determined to have the highest dilution without growth. Aliquots (10 μL) from wells with no growth were plated onto MHA and further incubated overnight at 37°C for the MBC test [33]. The MBC represented the highest dilution without surviving bacteria. Sterile water was utilized in place of NE for controls in both techniques and plating growth from wells was conducted to confirm culture purity.

2.9. Measurements of, nucleic acid, protein, and potassium leakage

By measuring the absorption of released genetic materials at 260 nm and 280 nm [34], the integrity of the cell membrane of *S. aureus* was evaluated. The release process of potassium ions, proteins, and nucleic acids in the conventional approach was based on a modified method described by Nejabatdoust et al. as follows: Fresh bacterial cultures were initially suspended in MHB (OD_{600} = 0.4–0.6). Then, Berberine/SKEO NE and SKEO NE were mixed with bacterial suspension (*S. aureus*) to achieve final concentrations of 0.8 mg/mL and 3.2 mg/mL, respectively. Sample tubes were shaken at 250 rpm and incubated at 37°C. After a 6-h incubation period, a predetermined volume of solution was extracted and centrifuged for 10 min at 4000 rpm. The supernatant was separated for protein and nucleic acid optical density (OD) measurements at 260 and 280 nm.

An atomic absorption spectrophotometer (Analytik Jena, ContrAA700, Jena, Germany) was utilized to determine the potassium concentration in the solution after the interaction between the bacteria and samples in the microfluidic system. The quantity of released potassium was subsequently measured using an atomic absorption spectrophotometer equipped with a potassium hollow

cathode lamp with a wavelength of 766.5 nm, a bandpass of 0.5 nm, and an air-acetylene flame. The absorbance values obtained were converted to K^+ concentration (ppm) by comparing them to a curve previously established using standard potassium ion solutions at 0, 1.5, 3, 5, 7, and 10 ppm [35,36].

2.10. Time-killing and growth inhibition curves

Using the time-kill approach, the viability of *S. aureus* bacteria in the presence of nanoemulsions was investigated. A suspension of pathogens was added to tubes containing the sterilized substance at MIC, resulting in a final bacterial concentration in a broth of 4.5–5.5 × 10^5 CFU/mL. After adding the substance, the tubes were incubated at 37°C, and viable counts were carried out 6 h later. All that was present in the control was MHB and bacteria. Conversely, at the designated residence period, 5 mL of the bacterial solution was injected into the microfluidic and combined with the nanoemulsion at different concentrations. A serial dilution approach was used for evaluation, and a normal saline solution (0.085%) was present. Following the removal of 100 μL portions from each tube, the CFU was counted after a 24-h culture period at 37°C [37].

The following formulas were employed to calculate the inhibition and viability of bacterial cells:

$$\text{Percentage of viability} = \frac{\text{Number of colonies counted}}{\text{Number of control colonies}} \times 100 \quad (2)$$

$$\text{Percentage of inhibition} = 100 - \text{viability Percentage} \quad (3)$$

2.11. The morphological changes by SEM analysis

SEM was utilized to observe morphological changes and the appearance of cells treated with nanoemulsions [38]. After 20 min of bacterial treatment with Berberine/SKEO NE in the microfluidic system, the morphological change in the cell surface was observed by scanning electron microscopy. The bacterial cells were kept stable at room temperature for the duration of the night using 2.5% glutaraldehyde. After that, the cells were twice washed with PBS. The samples were dehydrated by varying amounts of ethanol (70%, 80%, 90%, and 100%). The dried cell samples were coated with 10 nm gold in a sputter coater, and SEM was used to scan them.

3. Results and discussion

3.1. Optimization of nanoemulsion formulation

BBD, one of the subclasses of RSM, was used to optimize independent parameters of nanoemulsion formulation. Based on the droplet size of the nanoemulsion, which exhibited the highest biological response and stability (Table S1, Supporting Information), the percentages of surfactant (A), essential oil (B), and chitosan (C) were optimized. The droplet size of the nanoemulsion was studied as a single response and recorded using the DLS technique.

The BBD plot consists of 17 runs, incorporating five center points (Table S1, Supporting Information). As a function of the independent parameters, actual and coded values of the droplet size are utilized to assess correlations in equations (4) and (5):

Table 1
ANOVA results for independent variables obtained from RSM.

Source	Sum of squares	Degree of freedom	Mean square	F-value	p-value Prob > F
Model	482.91	9	53.66	230.39	<0.0001 *significant.*
A-Surfactant	9.03	1	9.03	38.78	0.0004
B-Essential Oil	1.45	1	1.45	6.24	0.0411
C-Berberine	0.85	1	0.85	3.66	0.0975
AB	0.64	1	0.64	2.75	0.1413
AC	6.25	1	6.25	26.84	0.0013
BC	0.39	1	0.39	1.68	0.2364
A^2	73.52	1	73.52	315.69	<0.0001
B^2	33.99	1	33.99	145.95	<0.0001
C^2	319.89	1	319.89	1373.51	<0.0001
Residual	1.63	7	0.23		
Lack of fit	0.99	3	0.33	2.07	0.2464 *not significant.*
Pure error	0.64	4	0.16		
Core total	484.54	16			

$$\text{Droplet size of nanoemulsion (Actual)} = \text{Mean droplet size} = +316.22344 - 12.67812 \times \text{Surfactant} - 23.40625 \times \text{Essential Oil} - 3688.93750 \times \text{Berberine} - 0.20000 \times \text{Surfactant} \times \text{Essential Oil} + 31.25000 \times \text{Surfactant} \times \text{Berberine} + 15.62500 \times \text{Essential Oil} \times \text{Berberine} + 1.04469 \times \text{Surfactant}^2 + 2.84125 \times \text{Essential Oil}^2 + 21790.62500 \times \text{Berberine}^2 \quad (4)$$

$$\text{Droplet size of nanoemulsion (Coded)} = \text{Mean droplet size} = 88.63 - 1.06 \times A - 0.43 \times B + 0.33 \times C - 0.40 \times A \times B + 1.25 \times A \times C + 0.31 \times B \times C + 4.18 \times A^2 + 2.84 \times B^2 + 8.72 \times C^2 \quad (5)$$

The results of the ANOVA analysis of RSM are illustrated in Table 1. The statistical significance of the model was evaluated using the computed P-value index. In this study, a low p-value ($p < 0.0001$) and/or high F-value ($F = 230.39$) indicate the statistical significance of the model. Comparing the Lack of Fit index (0.2464) to the pure error also assesses how well the model fits the experimental data. Moreover, a determination coefficient (R^2) of 0.9966 demonstrates a meaningful correlation between experimental and predicted values in the model. Other key statistical features include a standard deviation of 0.48, coefficient of variation (C.V.%) of 0.50, adjusted R^2 of 0.9923, adequate precision of 40.205, and predicted R^2 of 0.9652. The proposed fitting model effectively predicts optimal and maximum biological response and stability conditions.

A figure depicting the discrepancies between the actual and projected results is also presented (Fig. S1A, Supporting Information). It aids in identifying values or data clusters the regression model cannot accurately predict. Moreover, these plots validate the consistency between predicted values and experimental data.

Furthermore, Fig. S1B in the Supporting Information displays plots of residuals versus fitted responses, which depict residuals against predicted response values.

It assesses the assumption of a constant variance. The plot should exhibit a random dispersion, maintaining a consistent residual

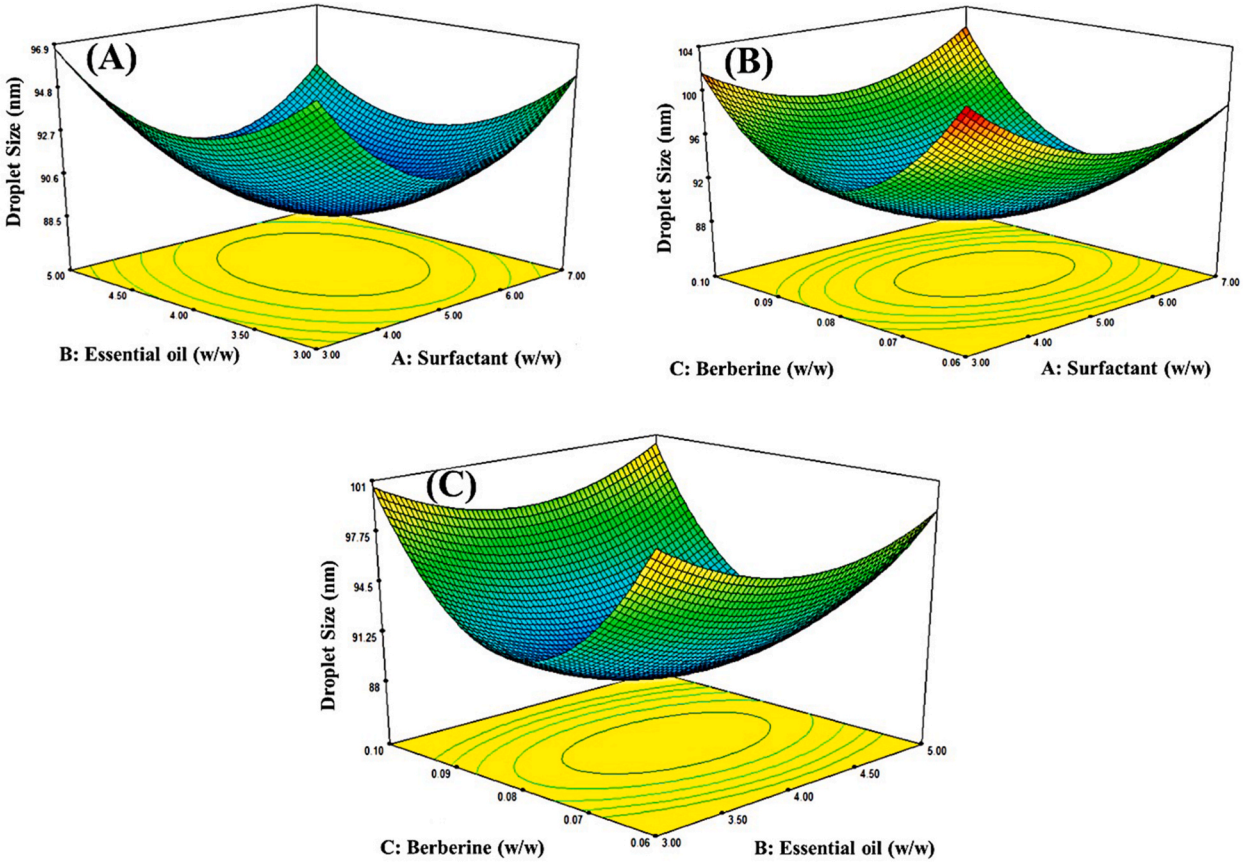

Fig. 2. Interaction effect of (A) surfactant and essential oil, (B) surfactant and Berberine, (C) Berberine and essential oil on the droplet size.

spread on the chart. The collected findings validate the precision of the proposed model. Fig. S1C in the supplementary information displays the variance between the predicted response and the actual data on the typical probability plot of the residuals. A typical probability plot suggests that data points should align along a straight line if the residuals adhere to a normal distribution (Fig. S1C, Supplementary Information).

3.2. Droplet size of nanoemulsion formulation factors interactive effect

The proportions of the nanoemulsion-forming components significantly impact the final droplet size. Previous studies suggest that a high proportion of surfactants could increase the toxicity of food and other products. Hence, adjustments were made to the percentages of chitosan, essential oil, and Tween 80 to attain the optimal droplet size for chitosan-based nanoemulsions. Given its low toxicity, minimal irritability, excellent stability, and ability to produce nanoemulsions with minimal droplet size, Tween 80 was selected as the surfactant.

Fig. 2 presents quadratic polynomial models' three-dimensional response surface contour plots, illustrating the interaction between independent and dependent variables. Fig. 2A depicts the influence of surfactant and essential oil percentages on the droplet size of Berberine/SKEO NE. As shown, the nanoemulsion droplet size initially experienced a slight decrease, followed by a notable increase, before eventually reaching a maximum with an escalation in the essential oil percentage while maintaining constant and low surfactant percentages. However, such growth was less prominent at higher surfactant levels.

Given that the ideal condition aims to achieve more stable nanodroplets with small particle sizes, the essential oil and surfactant may be selected from the middle portion of the curve.

Fig. 2B demonstrates how the concentration of Berberine and surfactant influences the droplet size of the Berberine/SKEO NE. It can be observed that initially increasing the Berberine factor to the middle range while keeping surfactant levels constant results in a reduction in droplet size, followed by a more significant increase in droplet size with further increases in Berberine amount. This plot implies the interaction effect between these two variables, as indicated in Table 1. Conversely, variations in surfactant levels at constant Berberine concentrations show a similar trend to the explanation provided in the previous figure, albeit with a less steep decline. Surfactants, comprising hydrophobic and hydrophilic structures, typically reduce interfacial tension at the oil-water interface, bridging the gap between the oil and aqueous phases. As a result, less free energy is required for nanoemulsion formation.

Consequently, increasing the Tween 80 concentration to the optimal middle range may reduce droplet size. According to Fig. 2B, increasing the Tween 80 content to the optimal middle range could reduce droplet sizes at constant Berberine amounts. However, a more significant increase depicts a contrary effect.

The impact of Berberine and essential oil on the average droplet size of a nanoemulsion is evident in Fig. 2C. The curve in the figure unequivocally illustrates that, at constant percentages of Berberine, the droplet size initially decreases as the amount of essential oil is increased to the middle range, and then it starts rising with the same slope. However, at constant essential oil percentages, variations in the amount of Berberine significantly impact the droplet size with notable changes. Additionally, the computed p-values in Table 1 confirm the statistical significance of the influence of the independent variables.

3.3. The optimization of droplet size

The optimal conditions for the selected variables were determined using the regression model. Three different case studies were conducted to validate the accuracy of the fitted relationship Table 2. Using Dynamic Light Scattering (DLS) (Nanophox Sympatec GmbH, Claushtal, Germany), the mean particle diameters of the nanoemulsions were 96.57 ± 4.6 nm, 88.60 ± 5.2 nm, and 93.52 ± 4.7 nm (Fig. 3A-C).

After 65 days of storage at 4°C, it was observed that the mean particle diameter remained relatively unchanged, indicating long-term storage stability (Fig. 4). Moreover, the polydispersity index (PDI) of the optimized three nanoemulsions was determined to be 0.18, 0.13, and 0.12, which is a crucial parameter for assessing the stability and quality of nanoemulsions. It measures the distribution of particle sizes in the emulsion.

Fig. 5(A, C, and E) displays the morphology of the generated nanoemulsions using TEM for optimum points No. 1, 2, and 3 which appeared spherical and homogeneous, with droplet sizes of 96.57, 88.60, and 93.52 nm respectively (Fig. 5(B, D, and F)). The DLS approach was also employed to measure droplet size for all three optimum points, yielding between 88.60 and 96.57 nm.

3.4. MIC and MBC for Berberine/SKEO NE

Table 3 presents the MIC and MBC values for Berberine, SKEO NE, and Berberine/SKEO NE at their optimal formulations (No.1,

Table 2
The optimal points chosen for nanoemulsion samples validation.

No.	*Surfactant* (w/w%) A	Essential Oil (w/w%) B	Berberine C (w/w%)	Predicted Droplet size (nm)	Reported Droplet size (nm)	Desirability
1	5.86	3.31	0.06	95.47	96.57 ± 4.6 nm	1.000
2	6.21	3.91	0.08	89.60	88.60 ± 5.2 nm	1.000
3	5.63	3.65	0.07	90.37	93.52 ± 4.7 nm	1.000

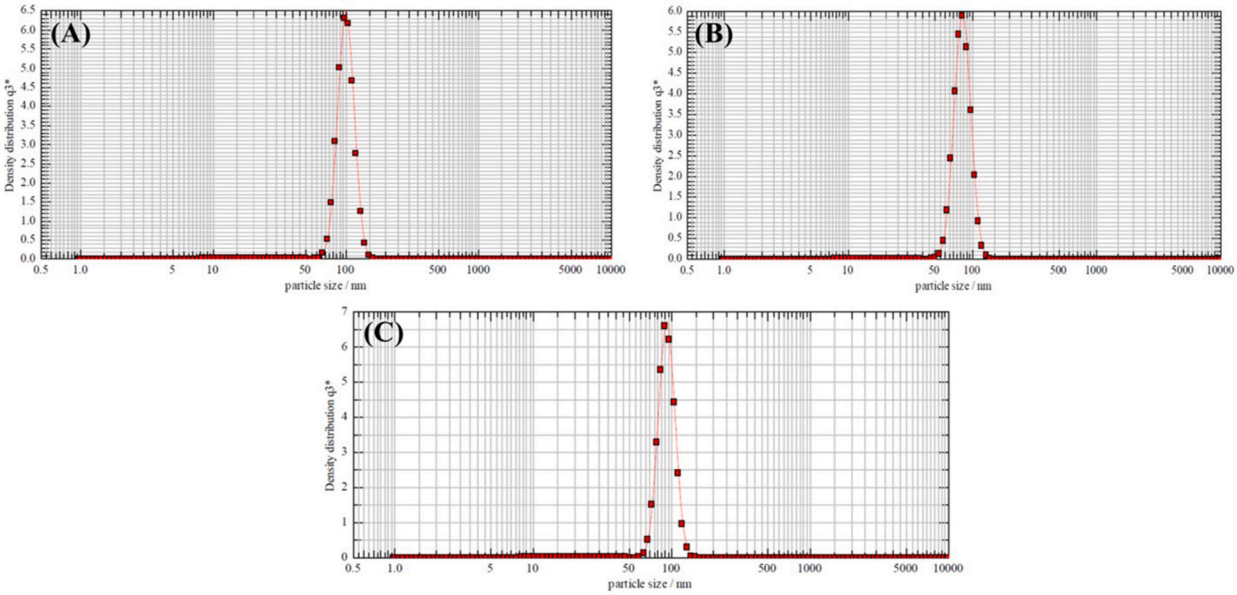

Fig. 3. The mean droplet size of the optimum point established using DLS were (A), No.1: 96.57 ± 4.6 nm, (B) No.2: 88.60 ± 5.2 nm, and (C) No.3: 93.52 ± 4.7 nm.

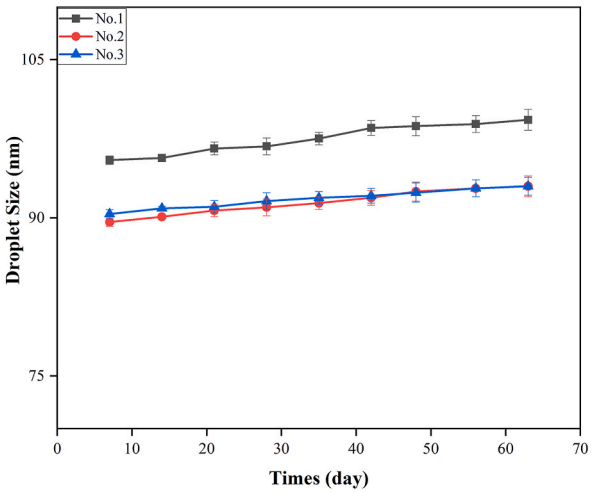

Fig. 4. Size changes assessment for the stability observations of the optimum points after 65 days.

No.2, and No.3) against *S. aureus* bacteria. Berberine/SKEO NE exhibits significantly higher antibacterial activity than separate samples of SKEO and Berberine. Moreover, it is worth mentioning that no significant differences in the bacterial inhibition were observed for the nanoemulsions at optimal points 2 and 3, while the optimized No. 1 demonstrated higher MIC which shows lower antibacterial efficiency. However, the optimized No. 2, and 3 Berberine/SKEO NE demonstrated greater antimicrobial efficacy against *S. aureus* bacteria. Between these two nanoemulsions, No. 2 was considered the best nanoformulation because of the same MIC and MBC values and lowest droplet size, resulting in higher interaction between the nanoemulsion and the bacterial cell due to an increased droplet surface area to the volume. Subsequently, femtosecond laser pulses were employed to weaken the bacterial cell wall, facilitating enhanced interaction between the bacteria and nanoemulsion to improve efficiency.

3.5. Membrane surgery to increase effectiveness using femtosecond laser

First, we use the optical tweezer to trap the *S. aureus* bacterium, enabling visualization of any morphological alterations induced by the nanoemulsion and real-time detection of bacterial destruction by the nanoemulsion. Fig. 6 presents optical microscope images captured upon adding the nanoemulsion to the bacteria trapped by the optical tweezers, along with subsequent photos taken at 3-, 5-,

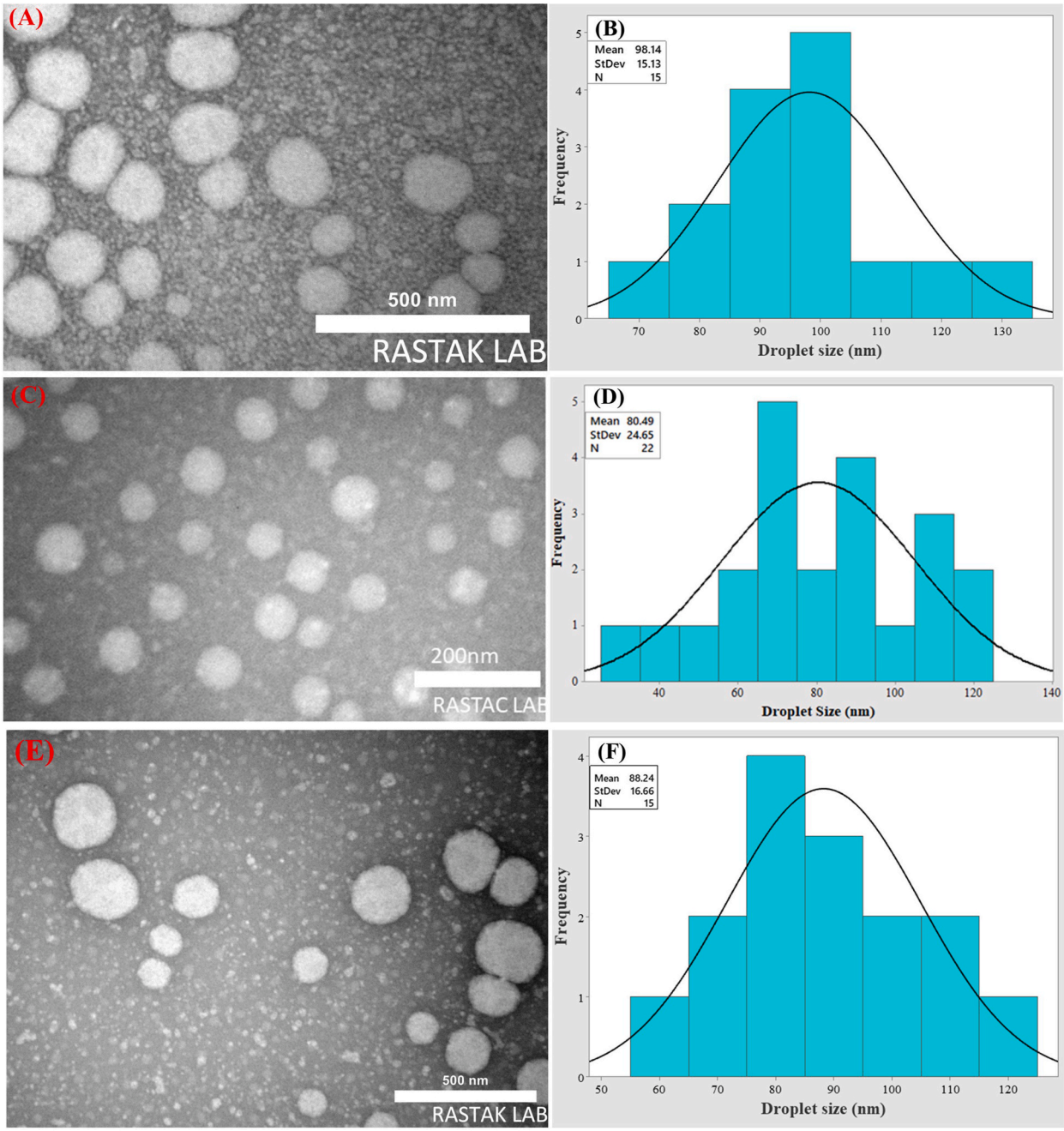

Fig. 5. TEM images for morphological measurement of nanoemulsions No. 1,2, and 3 (A, C, E respectively) and number frequency histograms to show the droplet size distribution of the nanoemulsion on a linear scale of 98.14, 80.49, and 88.24 nm (B, E, F).

10-, 15-, and 20-min intervals, respectively (Fig. 6A-F). A 36.8 mW power of the diode laser at 980 nm after passing through the optical and objective parts was employed to establish a stable optical trap of the bacteria, demonstrating relatively low absorption for biological specimens. The figure illustrates the progression of bacterial destruction following the addition of nanoemulsion over time, with evidence of bacterial degradation observed as early as 3 min, ultimately resulting in complete bacterial destruction by the 20-min mark.

The findings align perfectly with those of previous experiments. After 20 min of nanoemulsion treatment, the bacterium undergoes shape changes, as evidenced by microscopic photos, yet remains intact, consistent with the findings of this test. Moreover, it underscores the greater resilience of Gram-positive bacteria compared to Gram-negative bacteria, as observed in our prior research [39]. The reason could be that Gram-negative bacteria exhibit higher susceptibility, likely due to the primary components of essential oils

Table 3
S. aureus bacterium MIC and MBC results (mg/mL).

Compounds	Diameter (nm)	PDI	MIC	MBC
No.1	96.57	0.18	1.6	1.6
No.2	88.60	0.13	0.8	0.8
No.3	93.52	0.12	0.8	1.6
SKEO NE	99.56	0.14	3.2	3.2
SKEO	–	–	16.0	16.0
Berberine	–	–	16.0	32.0

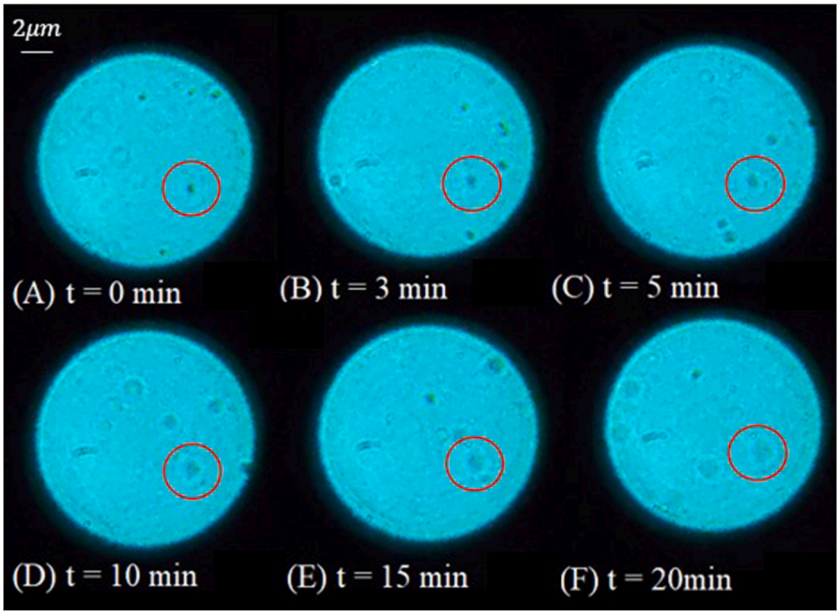

Fig. 6. Effect of nanoemulsion at different times, A) control, B) 3, C) 5, D) 10, E) 15, and F) 20 min on *S. aureus* bacterium trapped by optical tweezers at C = 250 μg/mL.

targeting both their inner and outer membranes. A more potent bactericidal effect is achieved by disrupting the cytoplasmic membrane, leading to cytoplasm leakage upon outer membrane damage.

Femtosecond laser pulses were employed to enhance the antibacterial efficacy of nanoemulsions. These ultra-short pulses non-invasively stimulate the surface of the membrane layer, expediting the interaction process between Berberine/SKEO NE and the bacterial cell membrane. Here, we investigated the irradiation of a femtosecond laser with a wavelength of 1040 nm and a pulse duration of 200 fs onto the bacterial surface. Ultra-short pulses with a power of 14.3 mW were utilized to manipulate the membrane layer. Fig. 7A (t = 0 min) shows bacteria trapped after irradiation with an ultrashort pulse for 40 s. The femtosecond pulse radiation induces surface stimulation of the bacterial membrane, creating pores on the cell wall. This phenomenon enhances cell permeability, facilitating the rapid entry of nanoemulsion materials into the bacterial cytoplasm.

Consequently, it accelerates the degradation process. A more rapid rupture of the *S. aureus* bacterial cell membrane is evident in Fig. 7, resulting in the discharge of cellular contents. The degradation process is observable at 3, 6, and 9 min in Fig. 7B-D compared to the state before femtosecond pulse irradiation in Fig. 6.

In the above experiments, it is crucial to demonstrate that the femtosecond laser with an energy of 0.62 nJ per pulse alone cannot destroy bacterial cells. To be confirmed, bacterial cells were illuminated by femtosecond laser pulses for 40 s without nanoemulsion, at the beginning (t = 0 min) (Fig. S2A) and 5-, 15-, and 20-min intervals, respectively, as depicted in Figs. S2(B–D). As observed, there was no destruction or deformation of the cells. Incorporating laser pulses led to an approximate 15% increase (Fig. 8C) in bacterial cell inhibition at the maximum concentration after 40 s of laser pulse radiation, compared to the conventional method after 6 h of treatment. Similarly, at lower concentrations, there was a noticeable increase compared to the conventional module (Fig. 8A). Moreover, the inhibition percentage after 5 and 20 min of treatment was evaluated in the microfluidic system at a significantly shorter time than the conventional method which is considered to be more desirable. As demonstrated in Fig. 8B, especially after 20 min of treatment at the highest concentration (250 μg/mL), the inhibition rate has increased to around 53% compared to that of the conventional method (48%). On the other hand, it is worth mentioning that after incorporating the laser pulse, the inhibition percentage at the same concentration has been increased to around 60%, demonstrating a favorable result in an even shorter time (40 s). According

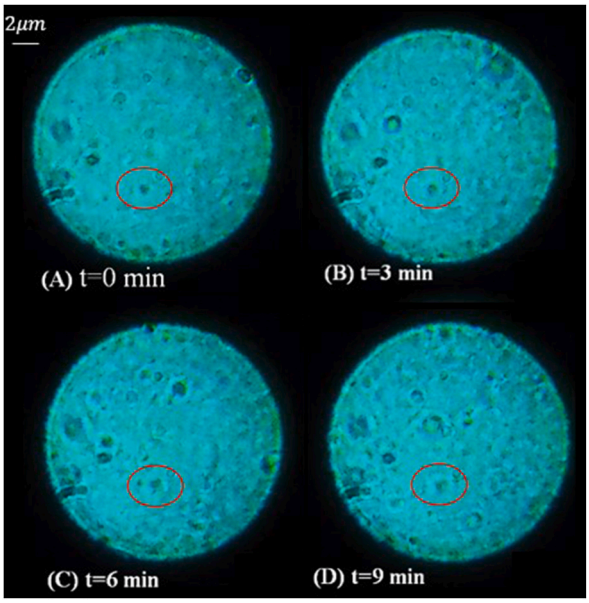

Fig. 7. Investigating the change of bacterial morphology at different times after treatment with nanoemulsion under femtosecond laser pulse irradiation for 40 s, A) control, B) 3, C) 6, and D) 9, min on *S. aureus* bacterium trapped by optical tweezers at C = 250 μg/mL.

to previous research, low-energy ultrashort pulses lack thermal effects and do not pose a thermal risk to bacterial life [40]. Femtosecond pulses, with their high peak power, can locally disrupt the arrangement of the bacterial membrane layer through nonlinear effects on the surface. This disruption creates penetration paths through which nanoemulsion enters the cytoplasm. Therefore, using femtosecond pulses can enhance the antibacterial effect of nanoemulsion materials.

For each bacterium, the combined treatment of the femtosecond laser and the nanoemulsions significantly enhanced the antibacterial effect of nanoemulsions, indicating the potential usefulness of this treatment to boost the antibacterial activity of nanoemulsions. Non-invasive manipulation of the bacterial surface by ultrashort pulses disrupts only the membrane layer, facilitating rapid entry of nanoemulsion material into the bacterial cytoplasm.

3.6. Antibacterial activity using the microfluidic and conventional methods

The inhibition rates (OD_{600}nm) of *S. aureus* bacteria using a microfluidic system are depicted in Fig. 9 at residence times of 5, 10, 15, and 20 min. The bactericidal activity was reduced by SKEO, SKEO NE, and Berberine/SKEO NE, with the latter exhibiting the most significant impact on inhibiting bacterial cell growth ($OD_{600nm} = 0.478$ for the control group) after 20 min of treatment but failing to suppress it entirely. The enhanced interaction of nanoemulsions with lipid membranes, more prevalent on the surface of Gram-negative bacteria than Gram-positive bacteria, is evident from a reference [41].

As indicated by the absorption at 260 and 280 nm, the interaction between the inhibitory agents and the bacterial membrane can release intracellular components such as K^+, DNA, RNA, and other materials [42]. Cell membrane damage is evidenced by the leakage of these components [43]. Utilizing a microfluidic system (Table S2 and Fig. S3) or conventional techniques to measure the levels of proteins and nucleic acids (MIC concentration), the antibacterial activity of the produced nanoemulsions against *S. aureus* was assessed. Nucleic acids and proteins are essential components of the cell, carrying genetic information and the foundation of life, respectively [44]. As shown in Table 4, the release of proteins and nucleic acids in *S. aureus* bacterium is higher for the sample incubated with Berberine/SKEO NE for 6 h, compared to the control and other samples. Fig. S3(A, B) depicts the evaluation of protein and nucleic acid release from different samples during a 20-min residence time in the microfluidic system. The maximum leakage observed was 0.785 and 0.662 in terms of OD_{260} nm and OD_{280} nm for *S. aureus*.

Another method of confirming the rupture of cell membranes was to measure the amount of potassium leakage. Table 4 displays the potassium leakage from the *S. aureus* bacteria after treatment using the traditional method for 6 h at MIC values. Potassium content was 0.28 ± 0.003 ppm for the control sample and increased to 0.626 ± 0.039, 0.587 ± 0.037, and 0.40 ± 0.005 ppm for the Berberine/SKEO NE, SKEO NE, and SKEO, respectively.

Fig. 10 illustrates the potassium release from different samples after treatment in a microfluidic system for 5, 10, 15, and 20 min at a 250 μg/mL concentration. The potassium leakage for the control group remained relatively constant at 0.35 ± 0.016 ppm. In contrast, this value increased to 0.654 ± 0.012 ppm for the sample treated with the Berberine/SKEO NE and SKEO NE, significantly surpassing that of the former sample ($p < 0.05$). This rise in concentration may be attributed to more significant damage to the cell wall and increased cell permeability. The results demonstrated enhanced antibacterial activity, suggesting a synergistic effect between both components of the nanoemulsion.

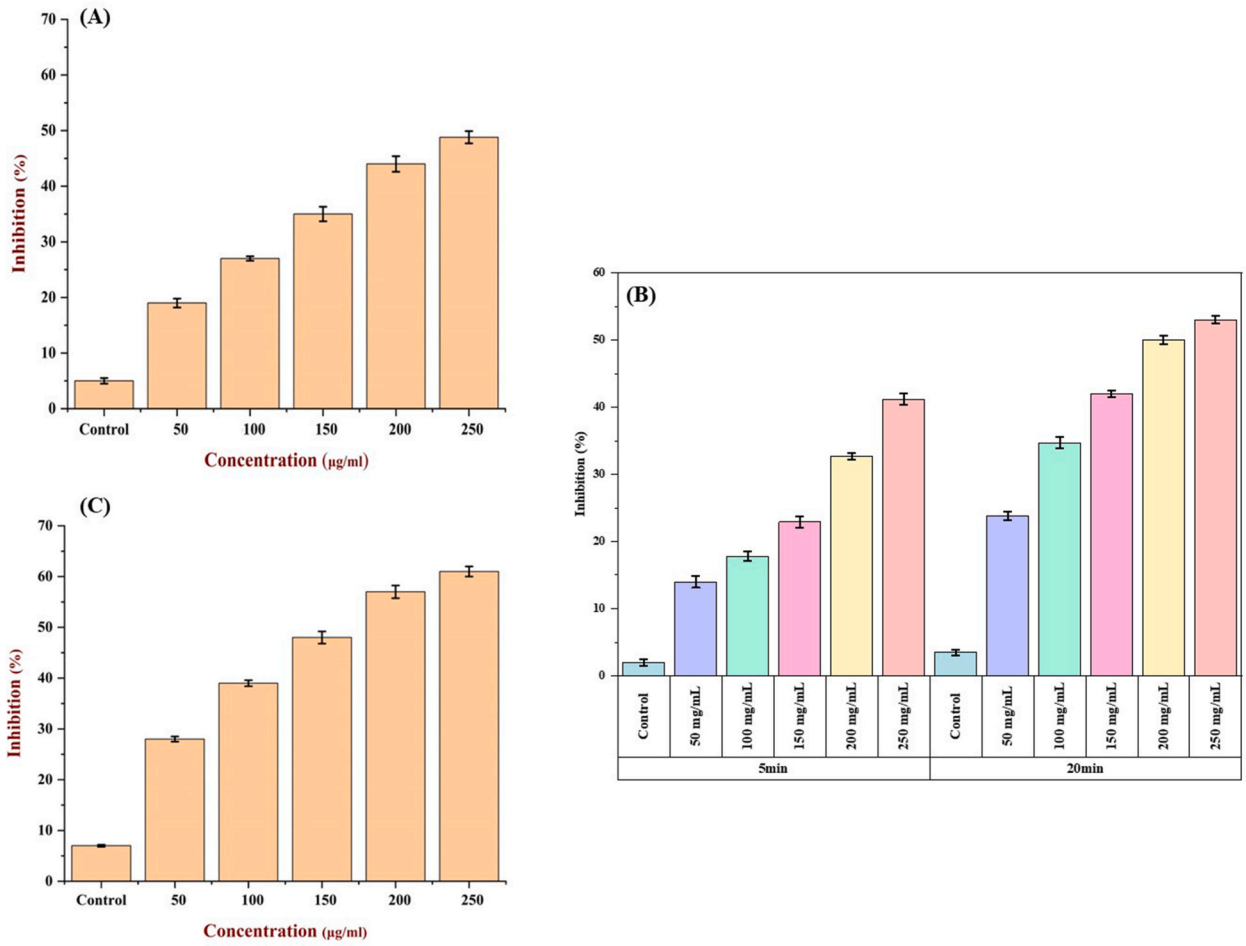

Fig. 8. Bacterial cell inhibition in the conventional method without incorporation of laser pulses (A), in a microfluidic system after 5 and 20 min of treatment (B), with laser pulses incorporation (C).

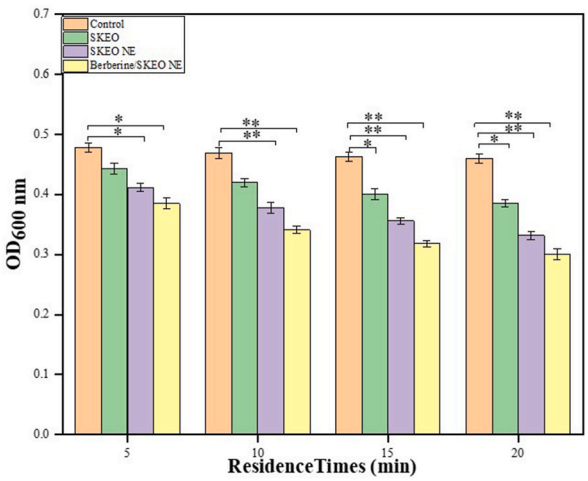

Fig. 9. *S. aureus* viability at different samples at 250 μg/mL and various residence times. The one-way ANOVA analysis signifies $p < 0.05$*, $p < 0.01$**, and $p < 0.001$*** compared with the control groups.

Table 4
Potassium leakage (mg/mL) from *S. aureus* bacterium after 6h operation.

Samples	Potassium leakage (mg/mL)
Control	0.28 ± 0.004
Berberine/SKEO NE	0.626 ± 0.039
SKEO	0.40 ± 0.005
SKEO NE	0.587 ± 0.037

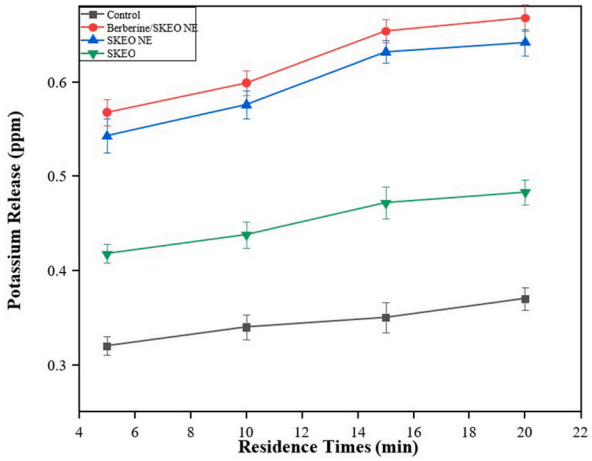

Fig. 10. The potassium release from various residence times and samples of the *S. aureus* bacterium indicated by a one-way ANOVA, signifies significant alterations ($p < 0.05$) when compared to the control group.

3.7. Scanning electron microscopy (SEM)

The SEM analysis was utilized to investigate the morphological changes in *S. aureus* bacterial cells treated with Berberine/SKEO NE at a concentration of 250 μg/mL for 5 and 20 min (Fig. 11). The morphology of *S. aureus* cells, as depicted in Fig. 11A, suggests that the bacteria maintain their structural integrity, including a smooth cell wall and intact plasma membrane envelope. However, as shown in Fig. 11B, after 5 min of treatment, the nanoemulsion begins to adhere to the *S. aureus* surface, resulting in minor cell morphological alterations. Subsequently, after 20 min of treatment, significant morphological changes occur due to the adhesion of the nanoemulsion to the bacterial cell wall, potentially leading to the formation of tiny pores (Fig. 11C).

4. Conclusion

This study emphasizes the importance of utilizing effective active chemicals and maximizing surface area contact through nano-emulsification and microfluidic principles to inhibit bacterial activity. The study used a highly efficient microfluidic system alongside the conventional approach to investigate the interaction between an optimized Berberine/SKEO NE formulation and the *S. aureus* bacterium. Bacterial phospholipid bilayer membranes interact with naturally occurring substances, resulting in cell lysis. It was observed that the antibacterial activity of Berberine/SKEO NE is inversely correlated with droplet size, indicating that smaller droplet-size nanoemulsions exhibit more significant antibacterial activity. This relationship may be attributed to the increased efficient surface area and the higher number of particles colliding with the cell surface. Moreover, the femtosecond laser pulse, in combination with optical tweezers, creates tiny pores on the bacterial cell wall, facilitating enhanced contact between the nanoemulsion and the cell wall. Illuminating by femtosecond lasers successfully accelerated the antibacterial activity of Berberine/SKEO NE against *S. aureus* bacteria, making them a potential technique for food preservatives.

Data availability

Data will be made available on request.

CRediT authorship contribution statement

Liana Parseghian: Investigation, Visualization, Validation, Formal analysis, Biological evaluation, Writing – original draft. **Nastaran Kahrarian:** Investigation, Visualization, Writing – original draft. **Atoosa Sadat Arabanian:** Conceptualization, Resources, Writing – Review & editing, Supervision. **Zinab Moradi Alvand:** Biological evaluation, Writing – original draft, Validation. **Reza**

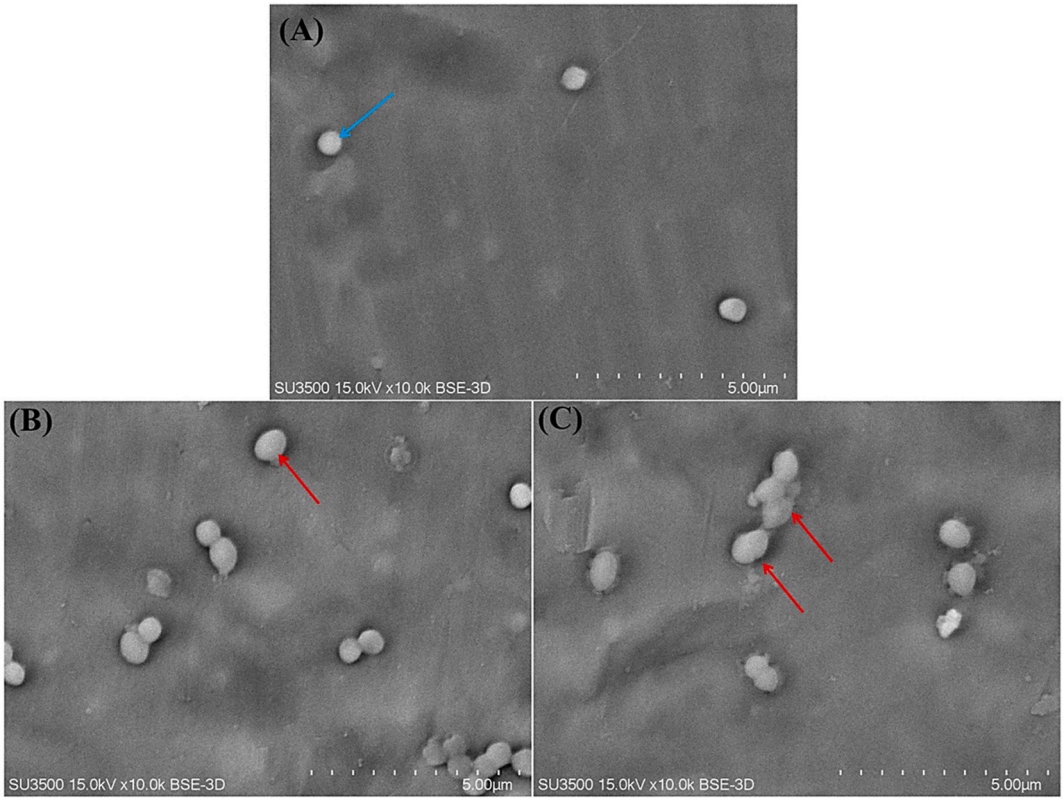

Fig. 11. SEM images of *S. aureus* bacterium cells treated with 250 µg/mL Berberine/SKEO NE using the microfluidic system. (A: Control, B, and C treated for 5 and 20 min).

Massudi: Writing – review & editing, Resources, Supervision, Validation. **Masoud Rahimi:** Formal analysis, Conceptualization. **Hasan Rafati:** Conceptualization, Resources, Writing – Review & editing, Supervision.

Declaration of competing interest

The authors declare that they have no known competing financial interests or personal relationships that could have appeared to influence the work reported in this paper.

Acknowledgments

The authors gratefully acknowledge the support provided by Shahid Beheshti University Research Council.

Appendix A. Supplementary data

Supplementary data to this article can be found online at https://doi.org/10.1016/j.heliyon.2024.e37283.

References

[1] S.K. Amit, M.M. Uddin, R. Rahman, S.M.R. Islam, M.S. Khan, A review on mechanisms and commercial aspects of food preservation and processing, Agric. Food Secur. 6 (2017) 1–22.
[2] T. Maho, R. Binois, F. Brulé-Morabito, M. Demasure, C. Douat, S. Dozias, P.E. Bocanegra, I. Goard, L. Hocqueloux, C. Le Helloco, I. Orel, J.M. Pouvesle, T. Prazuck, A. Stancampiano, C. Tocaben, E. Robert, Anti-bacterial action of plasma multi-jets in the context of chronic wound healing, Appl. Sci. 11 (2021), https://doi.org/10.3390/app11209598.
[3] M. Bondi, A. Lauková, S. de Niederhausern, P. Messi, C. Papadopoulou, Natural Preservatives to Improve Food Quality and Safety, vol. 2017, J Food Qual, 2017, pp. 1–3.
[4] Y. Herdiana, Functional food in relation to gastroesophageal reflux disease (GERD), Nutrients 15 (2023) 3583.
[5] E. Teshome, S.F. Forsido, H.P.V. Rupasinghe, E. Olika Keyata, Potentials of natural preservatives to enhance food safety and shelf life: a review, Sci. World J. 2022 (2022) 9901018.

[6] L. Geerlofs, Z. He, S. Xiao, Z.-C. Xiao, Efficacy of berberine as a preservative against mold and yeast in poultry feed, Approaches in Poultry, Dairy & Veterinary Sciences 6 (2019) 601–605.
[7] W. Mączka, M. Twardawska, M. Grabarczyk, K. Wińska, Carvacrol—a natural phenolic compound with antimicrobial properties, Antibiotics 12 (2023) 824.
[8] D.C. Dai ChunMei, P.C. Peng Cheng, W.J. Wang JiaBo, X.X. Xiao XiaoHe, Dose-effect Relationship of Berberine and Analogues on Antibacterial Metabolism of Bacillus Shigae by Microcalorimetry, 2010.
[9] X. Shang, C. Yang, S.L. Morris-Natschke, J. Li, X. Yin, Y. Liu, X. Guo, J. Peng, M. Goto, J. Zhang, Biologically active isoquinoline alkaloids covering 2014–2018, Med. Res. Rev. 40 (2020) 2212–2289.
[10] S. Wu, K. Yang, Y. Hong, Y. Gong, J. Ni, N. Yang, W. Ding, A new perspective on the antimicrobial mechanism of berberine hydrochloride against Staphylococcus aureus revealed by untargeted metabolomic studies, Front. Microbiol. 13 (2022) 917414.
[11] B. Salehi, Z. Selamoglu, B. Sener, M. Kilic, A. Kumar Jugran, N. de Tommasi, C. Sinisgalli, L. Milella, J. Rajkovic, M. Flaviana B. Morais-Braga, Berberis plants—drifting from farm to food applications, phytotherapy, and phytopharmacology, Foods 8 (2019) 522.
[12] M. Kaya, P. Ravikumar, S. Ilk, M. Mujtaba, L. Akyuz, J. Labidi, A.M. Salaberria, Y.S. Cakmak, S.K. Erkul, Production and characterization of chitosan based edible films from Berberis crataegina's fruit extract and seed oil, Innovat. Food Sci. Emerg. Technol. 45 (2018) 287–297.
[13] X. Liu, L. Chen, Y. Kang, D. He, B. Yang, K. Wu, Cinnamon essential oil nanoemulsions by high-pressure homogenization: formulation, stability, and antimicrobial activity, Lwt 147 (2021) 111660.
[14] S. Xia, L. Ma, G. Wang, J. Yang, M. Zhang, X. Wang, J. Su, M. Xie, In vitro antimicrobial activity and the mechanism of berberine against methicillin-resistant Staphylococcus aureus isolated from bloodstream infection patients, Infect. Drug Resist. (2022) 1933–1944.
[15] Z. Zhang, Y. Chen, J. Deng, X. Jia, J. Zhou, H. Lv, Solid dispersion of berberine–phospholipid complex/TPGS 1000/SiO2: preparation, characterization and in vivo studies, Int J Pharm 465 (2014) 306–316.
[16] W. Xu, P. Ling, T. Zhang, Polymeric micelles, a promising drug delivery system to enhance bioavailability of poorly water-soluble drugs, J Drug Deliv 2013 (2013) 340315.
[17] L. Taouzinet, O. Djaoudene, S. Fatmi, C. Bouiche, M. Amrane-Abider, H. Bougherra, F. Rezgui, K. Madani, Trends of nanoencapsulation strategy for natural compounds in the food industry, Processes 11 (2023) 1459.
[18] Y. Khan, H. Sadia, S.Z. Ali Shah, M.N. Khan, A.A. Shah, N. Ullah, M.F. Ullah, H. Bibi, O.T. Bafakeeh, N. Ben Khedher, Classification, synthetic, and characterization approaches to nanoparticles, and their applications in various fields of nanotechnology: a review, Catalysts 12 (2022) 1386.
[19] H. Zhang, J. Yang, R. Sun, S. Han, Z. Yang, L. Teng, Microfluidics for nano-drug delivery systems: from fundamentals to industrialization, Acta Pharm. Sin. B 13 (2023) 3277–3299.
[20] C. Arbore, L. Perego, M. Sergides, M. Capitanio, Probing force in living cells with optical tweezers: from single-molecule mechanics to cell mechanotransduction, Biophys Rev 11 (2019) 765–782.
[21] Z. Zhang, T.E.P. Kimkes, M. Heinemann, Manipulating rod-shaped bacteria with optical tweezers, Sci. Rep. 9 (2019) 19086.
[22] H. Zhang, K.-K. Liu, Optical tweezers for single cells, J R Soc Interface 5 (2008) 671–690.
[23] T.L. Min, P.J. Mears, L.M. Chubiz, C. V Rao, I. Golding, Y.R. Chemla, High-resolution, long-term characterization of bacterial motility using optical tweezers, Nat. Methods 6 (2009) 831–835.
[24] T. Kishimoto, K. Masui, W. Minoshima, C. Hosokawa, Recent advances in optical manipulation of cells and molecules for biological science, J. Photochem. Photobiol. C Photochem. Rev. 53 (2022) 100554.
[25] P.P. Lele, B.G. Hosu, H.C. Berg, Dynamics of mechanosensing in the bacterial flagellar motor, Proc. Natl. Acad. Sci. USA 110 (2013) 11839–11844.
[26] D. Malyshev, N.F. Robinson, R. Öberg, T. Dahlberg, M. Andersson, Reactive oxygen species generated by infrared laser light in optical tweezers inhibits the germination of bacterial spores, J Biophotonics 15 (2022) e202200081.
[27] A. Keloth, O. Anderson, D. Risbridger, L. Paterson, Single cell isolation using optical tweezers, Micromachines 9 (2018) 434.
[28] H.N. Banavath, S.R. Allam, S.S. Valathati, A. Sharan, B. Rajasekaran, Femtosecond laser pulse assisted photoporation for drug delivery in Chronic myelogenous leukemia cells, J. Photochem. Photobiol., B 187 (2018) 35–40.
[29] D. Goswami, Intense femtosecond optical pulse shaping approaches to spatiotemporal control, Front. Chem. 10 (2023) 1006637.
[30] Z.M. Alvand, M. Rahimi, H. Rafati, A microfluidic chip for visual investigation of the interaction of nanoemulsion of Satureja Khuzistanica essential oil and a model gram-negative bacteria, Int J Pharm 607 (2021) 121032.
[31] A. Jafarı-sales, B. Jafari, H. Khaneshpour, M. Pashazadeh, Antibacterial effect of methanolic extract of rosa damascena on standard bacteria Staphylococcus aureus, Bacillus cereus, Escherichia coli and Pseudomonas aeruginosa in vitro, International Journal of Nature and Life Sciences 4 (2020) 40–46.
[32] P. Parvekar, J. Palaskar, S. Metgud, R. Maria, S. Dutta, The minimum inhibitory concentration (MIC) and minimum bactericidal concentration (MBC) of silver nanoparticles against Staphylococcus aureus, Biomater Investig Dent 7 (2020) 105–109.
[33] S. Sepahvand, S. Amiri, M. Radi, H.-R. Akhavan, Antimicrobial activity of thymol and thymol-nanoemulsion against three food-borne pathogens inoculated in a sausage model, Food Bioproc Tech 14 (2021) 1936–1945.
[34] H. Yang, L. Song, P. Sun, R. Su, S. Wang, S. Cheng, X. Zhan, X. Lü, X. Xia, C. Shi, Synergistic bactericidal effect of ultrasound combined with citral nanoemulsion on Salmonella and its application in the preservation of purple kale, Ultrason. Sonochem. 92 (2023) 106269.
[35] M. Liu, Y. Pan, M. Feng, W. Guo, X. Fan, L. Feng, J. Huang, Y. Cao, Garlic essential oil in water nanoemulsion prepared by high-power ultrasound: properties, stability and its antibacterial mechanism against MRSA isolated from pork, Ultrason. Sonochem. 90 (2022) 106201.
[36] A. Nejabatdoust, H. Baghaei Daemi, A. Salehzadeh, S.C. Azimi, S. Darafkan, F. Fallah Digsara, M. Pourebrahim, R. Seighalani, Comparing of effects of hydro-alcoholic, ethanolic, and methanolic extracts of the Frangula alnus: chemical composition, antimicrobial, and synergism, Journal of Genetic Resources 6 (2020) 20–33.
[37] P.F. Xu, Z.H. Liu, Y.H. Duan, Q. Sun, D. Wang, X.F. Zeng, J.X. Wang, Microfluidic controllable synthesis of monodispersed sulfur nanoparticles with enhanced antibacterial activities, Chem. Eng. J. 398 (2020), https://doi.org/10.1016/j.cej.2020.125293.
[38] D. Liang, B. Feng, N. Li, L. Su, Z. Wang, F. Kong, Y. Bi, Preparation, characterization, and biological activity of Cinnamomum cassia essential oil nano-emulsion, Ultrason. Sonochem. 86 (2022) 106009.
[39] Z.M. Alvand, M. Rahimi, H. Rafati, Interaction of a natural compound nanoemulsion with Gram negative and Gram positive bacterial membrane; a mechanism based study using a microfluidic chip and DESI technique, Int J Pharm 626 (2022) 122181.
[40] I. V Ilina, D.S. Sitnikov, Application of ultrashort lasers in developmental biology: a review, in: Photonics, MDPI, 2022, p. 914.
[41] X. Liu, L. Chen, Y. Kang, D. He, B. Yang, K. Wu, Cinnamon essential oil nanoemulsions by high-pressure homogenization: formulation, stability, and antimicrobial activity, Lwt 147 (2021) 111660.
[42] C.Z. Chen, S.L. Cooper, Interactions between dendrimer biocides and bacterial membranes, Biomaterials 23 (2002) 3359–3368.
[43] I.-S. Woo, I.-K. Rhee, H.-D. Park, Differential damage in bacterial cells by microwave radiation on the basis of cell wall structure, Appl. Environ. Microbiol. 66 (2000) 2243–2247.
[44] V.K. Bajpai, A. Sharma, K. Baek, Antibacterial mechanism of action of T axus cuspidata stem essential oil against selected foodborne pathogens, J. Food Saf. 33 (2013) 348–359.